Enhanced biocatalytic degradation of lignin using combinations of lignin-degrading enzymes and accessory enzymes

Goran M.M. Rashid and Timothy D.H. Bugg*

Department of Chemistry, University of Warwick. Coventry CV4 7AL

Supporting Information

Figure S1. Gene cloning and protein purification of recombinant enzymes. A. *Agrobacterium* sp. DyP. B. *Comamonas testosteroni* DyP. C *Sphingobacterium* sp. T2. dihydrolipoamide dehydrogenase (DHLDH) DHLDH1 and DHLDH2. D. *Agrobacterium* sp. LigE.

Figure S2. pH/rate profiles of recombinant *Agrobacterium* DyP and *Comamonas testosteroni* DyP

Figure S3. Reaction of β-aryl ether lignin model compound guaiacylglyceryl-β-guaiacyl ether (GGE) with *Sphingobium* SYK-6 LigD and *Agrobacterium* sp. LigE, assessed by C18 reverse phase HPLC.

Figure S4. Reaction of *O*-benzylguaiacol (BnG) with *Agrobacterium* sp. LigE, assessed by C18 reverse phase HPLC.

Figure S5. Error analysis for data shown in Figure 2.

Figure S6. Calibration of FCA assay using vanillin as standard.

Figure S7. Reaction of organosolv lignin and β-aryl ether lignin dimer model compound with *Desulfitobacterium hafniense* arylsulfotransferase (AST)

Figure S8. Estimation of soluble lignin concentration by reaction with Coomassie dye G250

Figure S9. Increase in lignin solubility by treatment with *D. hafniense* AST

Figures S10-S19. New product peaks observed by reverse phase HPLC analysis of biotransformations of lignins by enzyme combinations.

Figures S20-S33. LC-MS data for new product peaks observed from biotransformation of lignins by enzyme combinations.

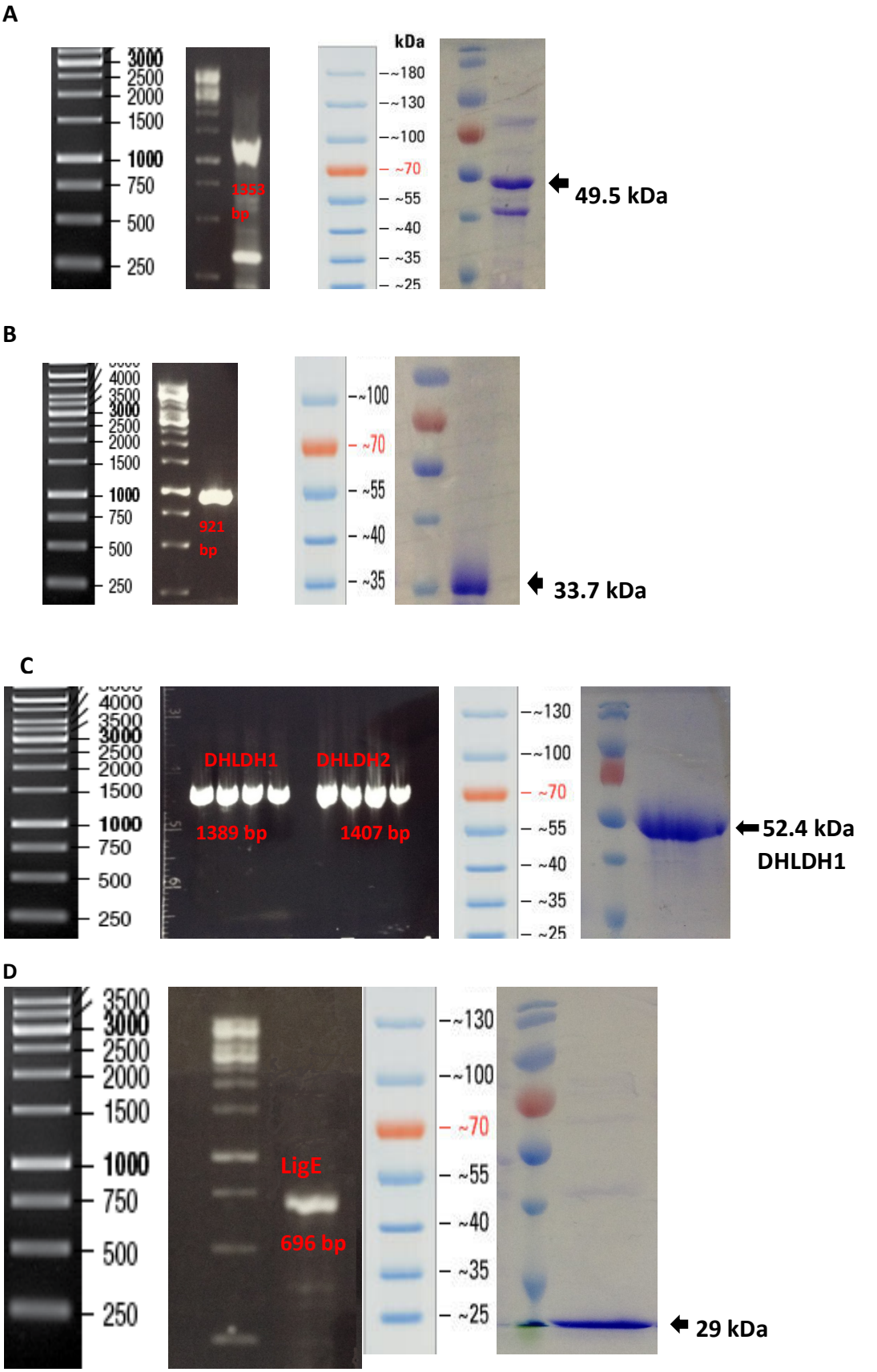

Figure S1. Gene cloning and protein purification of recombinant enzymes. A. *Agrobacterium* sp. DyP. B. *Comamonas testosteroni* DyP. C *Sphingobacterium* sp. T2. dihydrolipoamide dehydrogenase (DHLDH) DHLDH1 and DHLDH2. D. *Agrobacterium* sp. LigE.

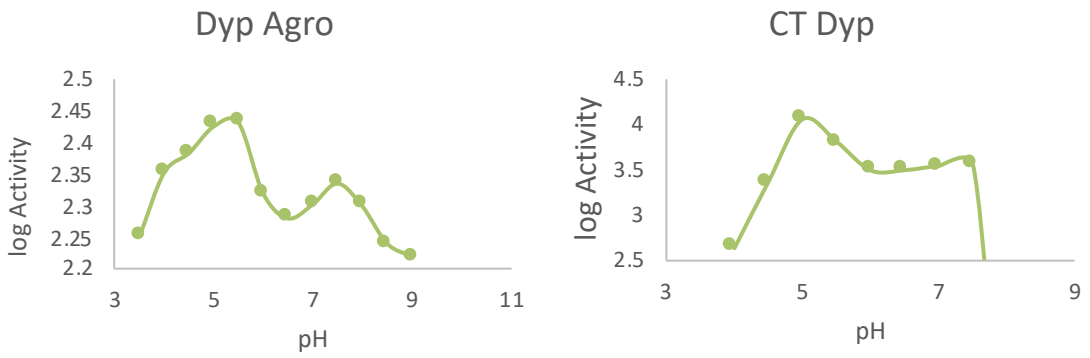

Figure S2. pH/rate profiles of recombinant Agro DyP and Ct DyP.

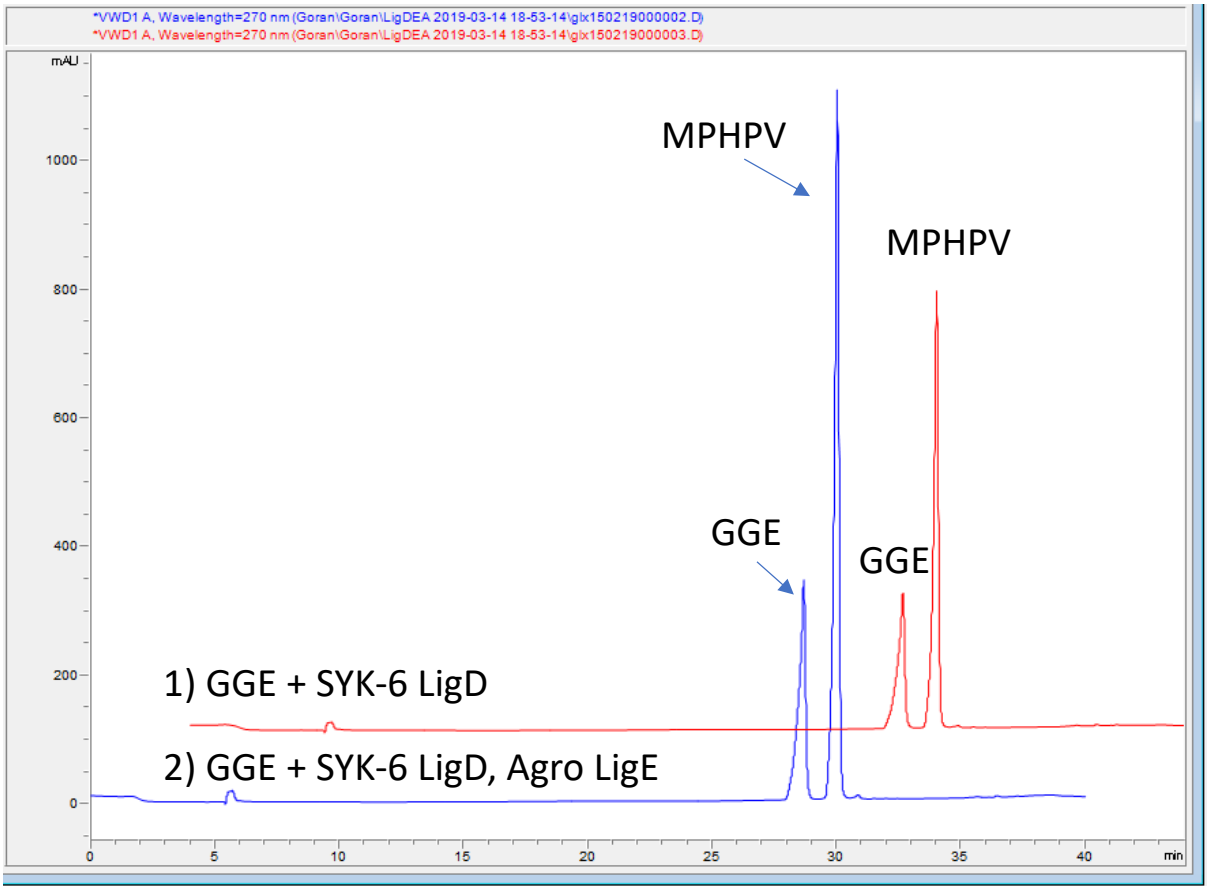

Figure S3. Reaction of β-aryl ether lignin model compound guaiacylglyceryl-β-guaiacyl ether (GGE) with *Sphingobium* SYK-6 LigD and *Agrobacterium* sp. LigE, assessed by C18 reverse phase HPLC. 1) incubation of GGE (1.0 mM) with 60 µg *Sphingobium* SYK-6 LigD and 1 mM NAD^+ (red); 2) incubation of GGE (1.0 mM) with 60 µg *Sphingobium* SYK-6 LigD and 100 µg *Agrobacterium* LigE in the presence of 1.0 mM NAD^+ and 1.0 mM glutathione (blue). The reactions were incubated for 16 hr at 30°C in 50 mM Tris-HCl buffer pH 8.0 containing 150 mM NaCl. MPHPV, α-(2-methoxyphenoxy)-β-hydroxypropiovanillone.

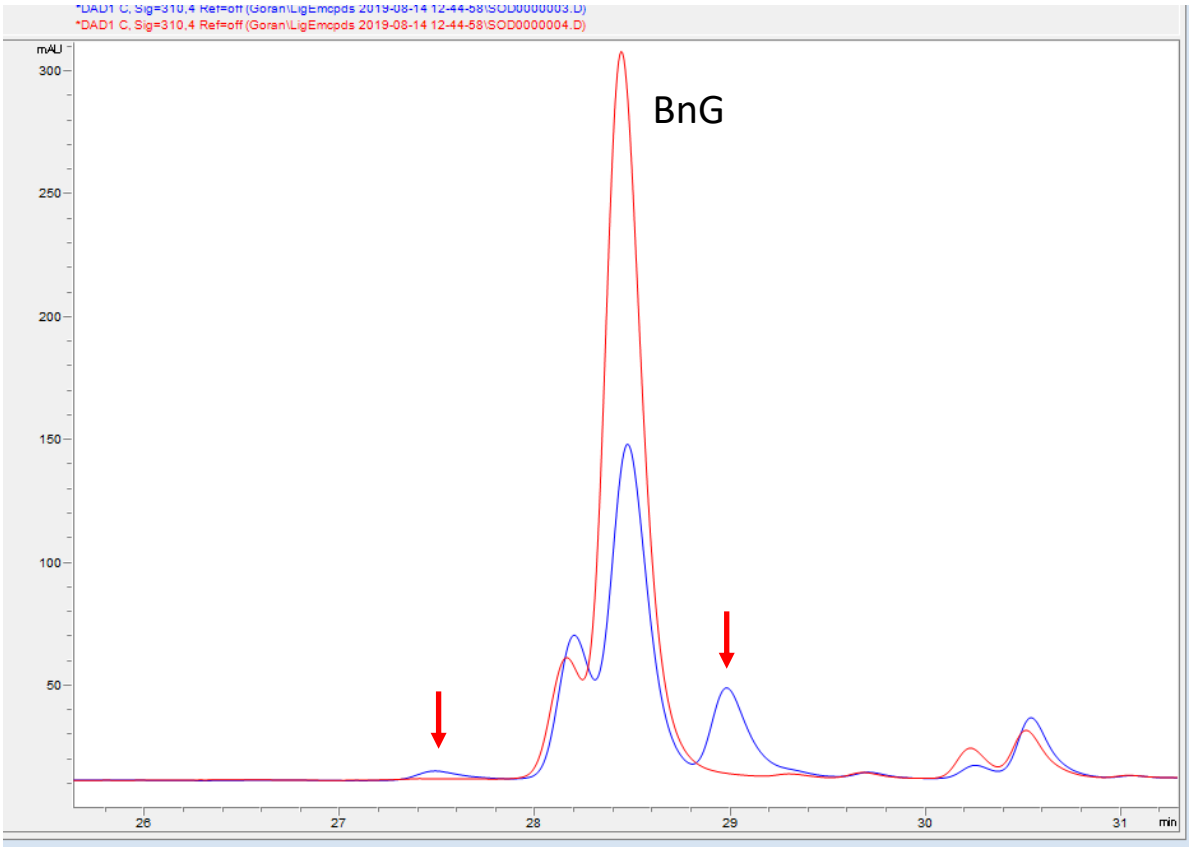

Figure S4. Reaction of *O*-benzylguaiacol (BnG) with *Agrobacterium* sp. LigE, assessed by C18 reverse phase HPLC. 1) Control sample of 100 µM BnG with 1 mM glutathione (red); 2) incubation of 100 µM BnG with 100 µg LigE in the presence of 1 mM glutathione (blue). Reactions were incubated at 30°C overnight in 50 mM Tris-HCl buffer pH 8.0 containing 150 mM NaCl. New peaks observed after reaction with LigE are marked with arrows.

	AV Humin				GVPL				AVL		
FCA HL 1 hr	A	N	CV	FCA hr	A	N	CV	FCA 1 hr	A	N	CV
A. DyP +DHLDH1	0.203	4	2.75%	A. DyP +DHLDH1	0.654	4	3.33%	A. DyP +DHLDH1	0.384	4	1.64%
Ct. DyP +DHLDH1	0.277	4	2.75%	Ct. DyP +DHLDH1	0.703	4	3.33%	Ct. DyP +DHLDH1	0.363	4	1.64%
DyP 1B +DHLDH1	0.272	4	4.61%	DyP 1B +DHLDH1	0.58	4	2.85%	DyP 1B +DHLDH1	0.306	4	5.44%
SOD1 +DHLDH1	0.257	4	3.61%	SOD1 +DHLDH1	0.391	4	2.85%	SOD1 +DHLDH1	0.305	4	5.44%
CopA	0.162	4	5.36%	CopA	0.348	4	2.44%	CopA	0.28	4	3.36%
O.CueO	0.172	4	5.36%	O.CueO	0.28	4	2.44%	O.CueO	0.342	4	3.36%
DHLDH1	0.104	4	4.16%	DHLDH1	0.287	4	1.71%	DHLDH2	0.244	4	0.93%
no Enz	0.178	4	3.16%	GV01	0.185	4	1.71%				
A. DyP +DHLDH2	0.271	4	2.10%	A. DyP +DHLDH2	0.894	4	5.28%	A. DyP +DHLDH2	0.518	4	0.95%
Ct. DyP +DHLDH2	0.3	4	2.10%	Ct. DyP +DHLDH2	0.793	4	5.28%	Ct. DyP +DHLDH2	0.438	4	0.95%
DyP 1B +DHLDH2	0.323	4	3.11%	DyP 1B +DHLDH2	0.723	4	2.87%	DyP 1B +DHLDH2	0.417	4	2.03%
SOD1 +DHLDH2	0.341	4	3.11%	SOD1 +DHLDH2	0.471	4	2.87%	SOD1 +DHLDH2	0.39	4	2.03%
CopA + DHLDH2	0.277	4	4.71%	CopA + DHLDH2	0.25	4	4.54%	CopA + DHLDH2	0.259	4	0.31%
O.CueO + DHLDH2	0.173	4	4.71%	O.CueO + DHLDH2	0.265	4	4.54%	O.CueO + DHLDH2	0.281	4	0.31%
DHLDH2	0.63	4	4.34%	DHLDH2	0.445	4	1.23%	DHLDH2	0.231	4	1.16%
no Enz	0.178	4	3.73%								
A. DyP +Prx	0.718	4	2.48%	A. DyP +Prx	0.698	4	2.81%	A. DyP +Prx	0.592	4	2.25%
Ct. DyP + Prx	0.664	4	2.48%	Ct. DyP + Prx	0.719	4	2.81%	Ct. DyP + Prx	0.401	4	2.25%
DyP 1B + Prx	0.801	4	3.16%	DyP 1B + Prx	0.488	4	1.56%	DyP 1B + Prx	0.467	4	3.35%
SOD1 + Prx	0.51	4	3.16%	SOD1 + Prx	0.377	4	1.56%	SOD1 + Prx	0.302	4	3.35%
CopA + Prx	0.231	4	3.42%	CopA + Prx	0.233	4	5.88%	CopA + Prx	0.219	4	2.27%
O.CueO + Prx	0.142	4	3.42%	O.CueO + Prx	0.308	4	5.88%	O.CueO + Prx	0.224	4	2.27%
Prx	0.229	4	2.47%	Prx	0.33	4	1.24%	Prx	0.246	4	2.13%
no Enz	0.178	4	2.47%								
A. DyP + Lig E	0.667	4	2.01%	A. DyP + Lig E	1.123	4	3.18%	A. DyP + Lig E	0.874	4	1.15%
Ct. DyP + Lig E	0.624	4	2.06%	Ct. DyP + Lig E	0.988	4	3.18%	Ct. DyP + Lig E	0.504	4	1.15%
DyP 1B + Lig E	0.732	4	2.17%	DyP 1B + Lig E	0.838	4	3.56%	DyP 1B + Lig E	0.55	4	1.38%
SOD1 + Lig E	0.387	4	2.17%	SOD1 + Lig E	0.342	4	3.56%	SOD1 + Lig E	0.329	4	1.38%
Lig E	0.266	4	5.92%	Lig E	1.2	4	1.45%	Lig E	0.741	4	0.76%
no Enz		4	2.92%								
A. DyP + AST	0.493	4	2.43%	A. DyP + AST	0.791	4	1.18%	A. DyP + AST	0.545	4	2.20%
Ct. DyP + AST	0.435	4	2.43%	Ct. DyP + AST	0.761	4	1.18%	Ct. DyP + AST	0.409	4	2.20%
DyP 1B + AST	0.428	4	1.22%	DyP 1B + AST	0.706	4	1.46%	DyP 1B + AST	0.376	4	1.36%
SOD1 + AST	0.436	4	1.22%	SOD1 + AST	0.571	4	1.46%	SOD1 + AST	0.389	4	1.36%
CopA + AST	0.329	4	3.94%	CopA + AST	0.663	4	2.02%	CopA + AST	0.28	4	1.19%
O.CueO + AST	0.359	4	3.94%	O.CueO + AST	0.543	4	2.02%	O.CueO + AST	0.342	4	1.19%

AST	0.318	4	2.00%	AST	0.682	4	1.02%	AST	0.218	4	2.72%
Control	0.112	4	2.00%					Control	0.227	4	2.72%
				CopA	0.324	4	0.17%				
				O.Cueo	0.255	4	0.17%	AST	0.263	4	0.57%

Figure S5. Error analysis for data shown in Figure 2, showing mean absorbance (A), number of replicates (N) and coefficient of variation (CV). Values of CV are typically 2-3%, with a maximum of 6%.

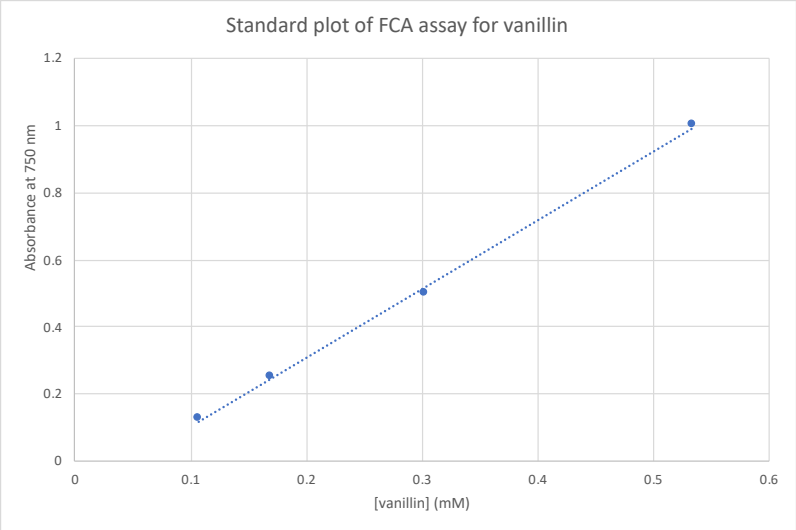

Figure S6. Calibration of FCA assay using vanillin as standard.

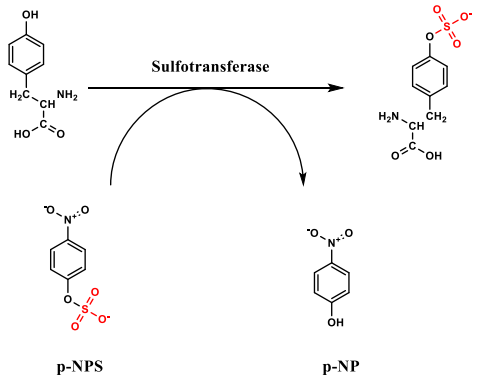

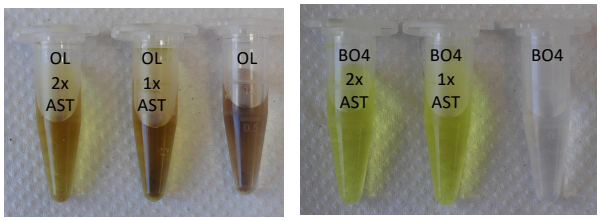

Incubation of organosolv lignin (OL) lignin and β-aryl ether lignin model compound (βO4) with arylsulfotransferase (AST) from *Desulfitobacterium hafniense*

Figure S7. Reaction of organosolv lignin and β-aryl ether lignin dimer model compound with *Desulfitobacterium hafniense* arylsulfotransferase (AST), generating p-nitrophenol by-product.

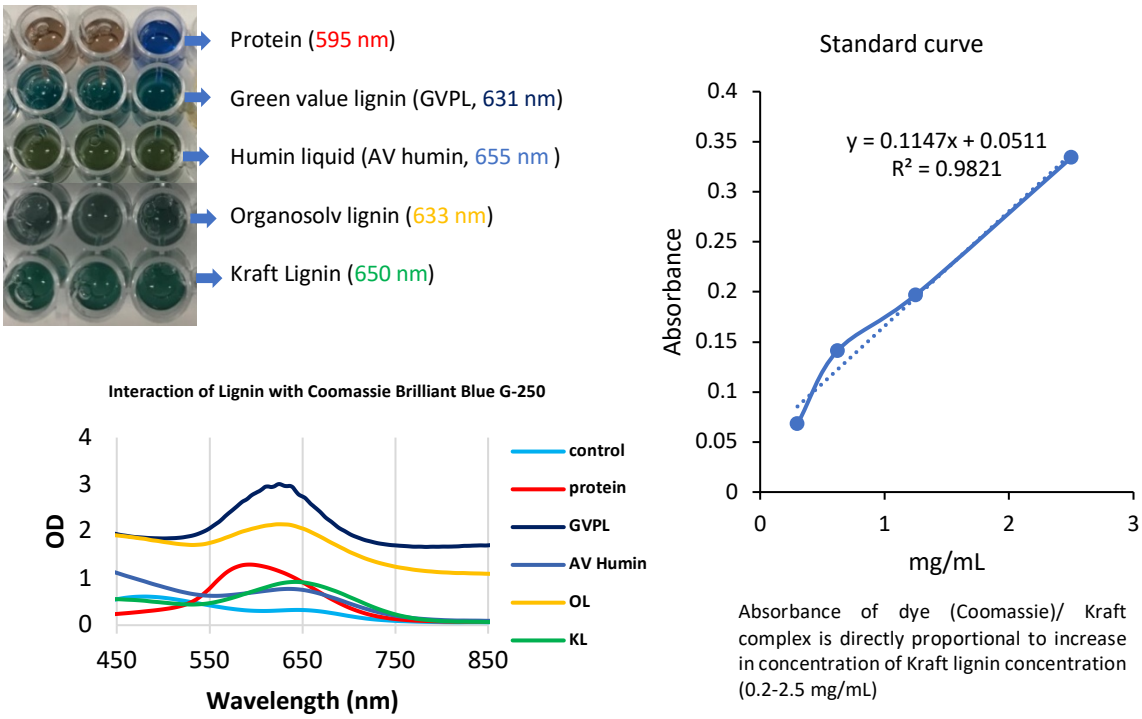

Figure S8. Estimation of soluble lignin concentration by reaction with Coomassie dye G250.

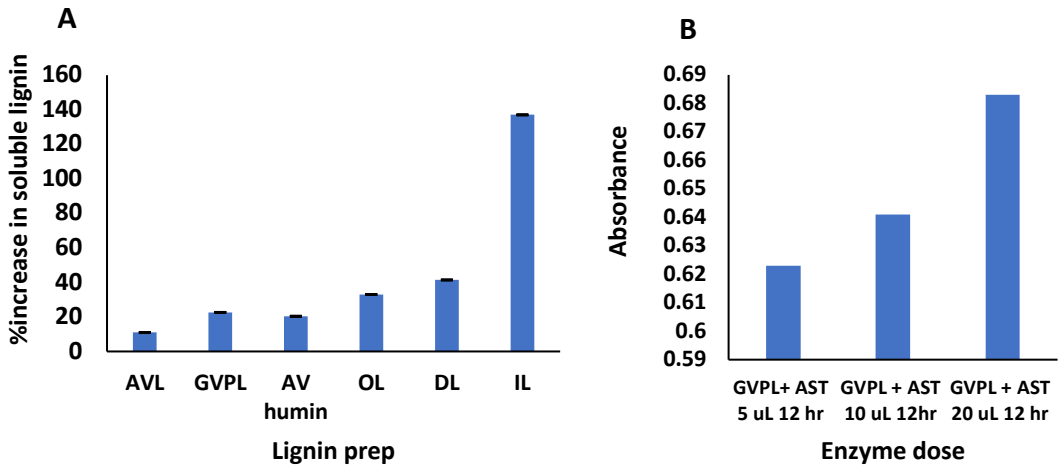

Figure S9. A. Percentage increase in soluble lignin by treatment with *D. hafniense* AST, estimated using Coomassie G250 dye. B. Increase in solubility of Green Value Protobind lignin correlates with dose of recombinant AST.

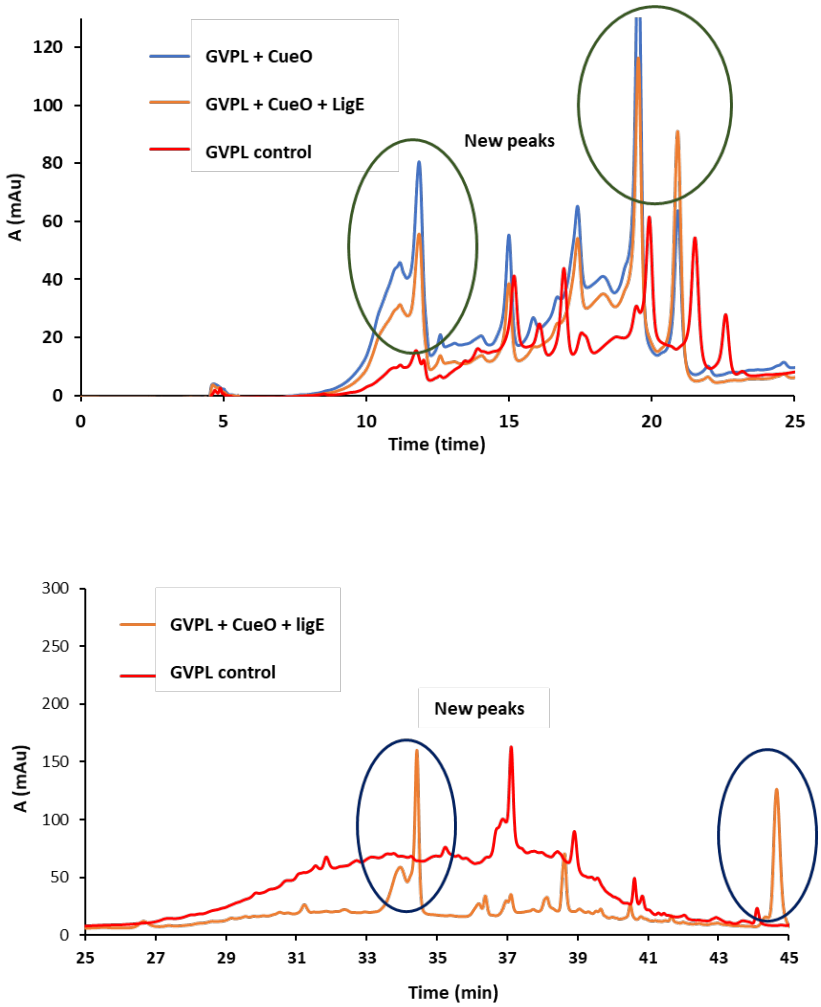

Figure S10. New product peaks from biotransformation of GVPL by Agro LigE in combination with CueO observed by reverse phase HPLC analysis (upper panel retention time 5-25 min, lower panel 25-45 min).

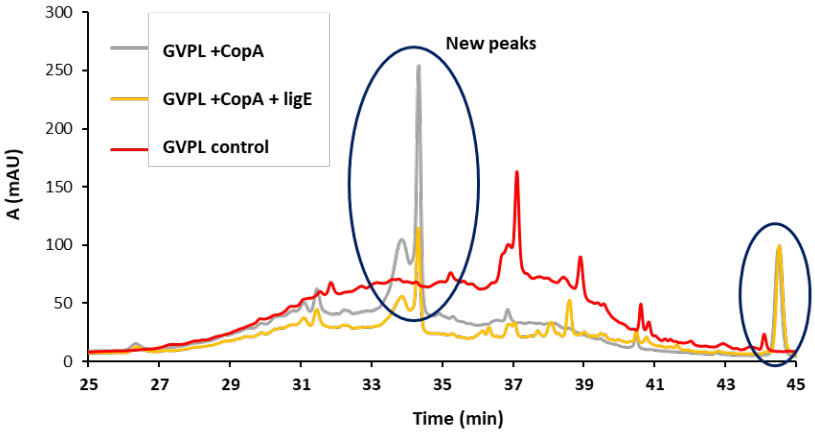

Figure S11. New product peaks from biotransformation of GVPL by Agro LigE in combination with CopA observed by reverse phase HPLC analysis.

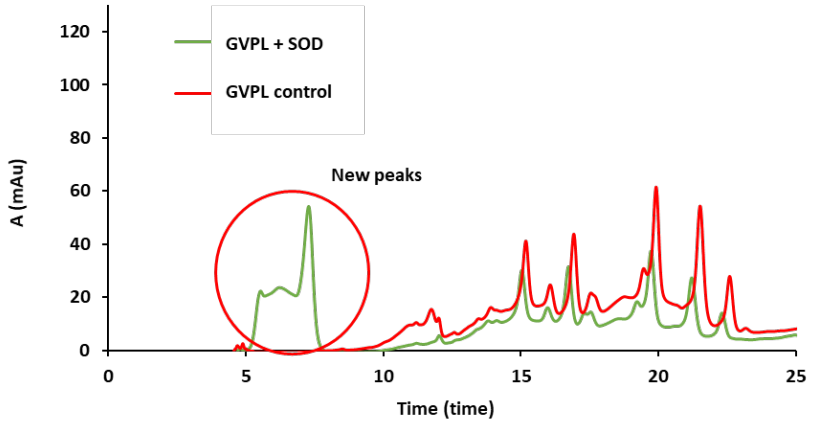

Figure S12. New product peaks from biotransformation of GVPL by *Sphingobacterium* MnSOD observed by reverse phase HPLC analysis.

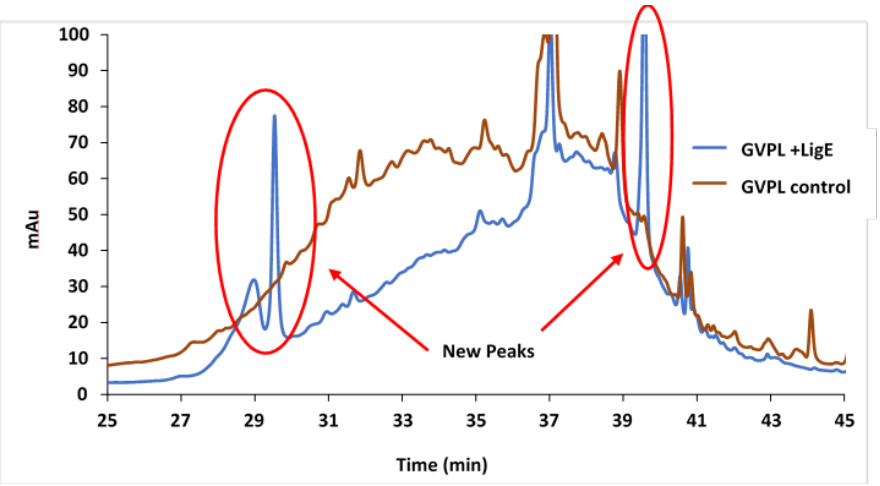

Figure S13. New product peaks from biotransformation of GVPL by Agro LigE observed by reverse phase HPLC analysis.

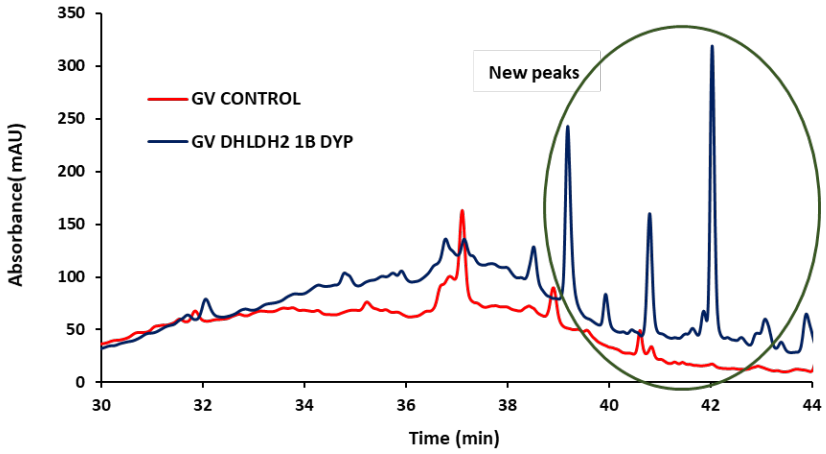

Figure S14. New product peaks from biotransformation of GVPL by *Sphingobacterium* DHLDH2 in combination with DyP 1B observed by reverse phase HPLC analysis.

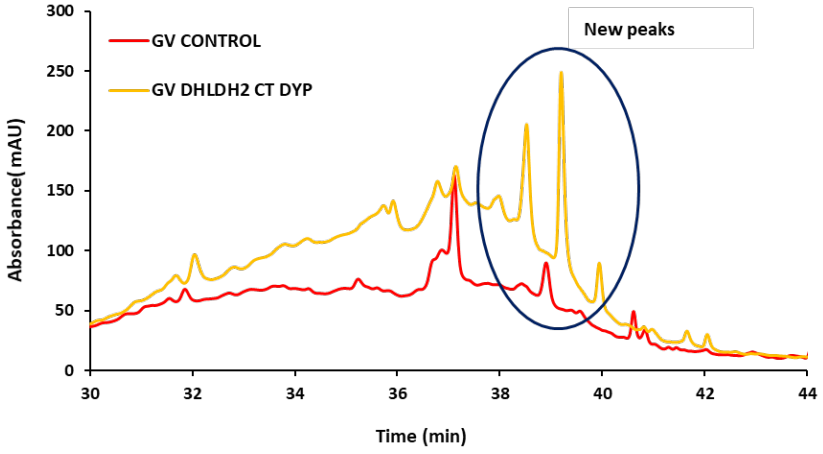

Figure S15. New product peaks from biotransformation of GVPL by *Sphingobacterium* DHLDH2 in combination with Ct DyP observed by reverse phase HPLC analysis

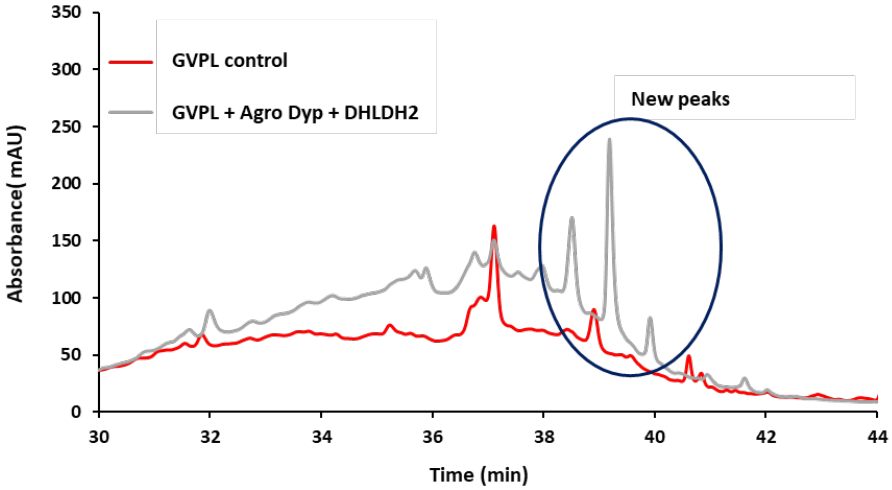

Figure S16. New product peaks from biotransformation of GVPL by *Sphingobacterium* DHLDH2 in combination with Agro DyP observed by reverse phase HPLC analysis.

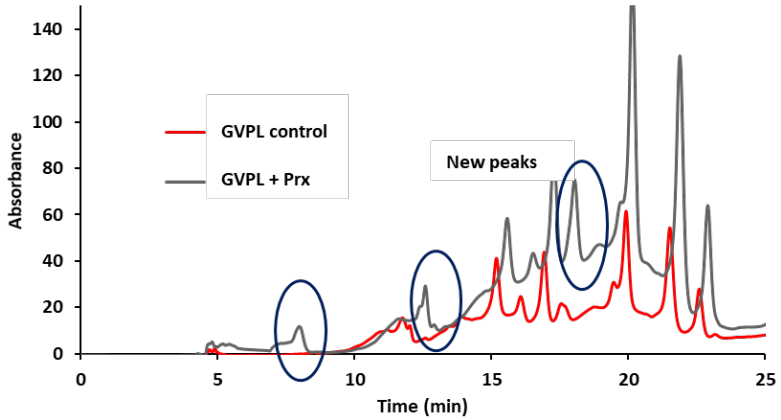

Figure S17. New product peaks from biotransformation of GVPL by Prx observed by reverse phase HPLC analysis.

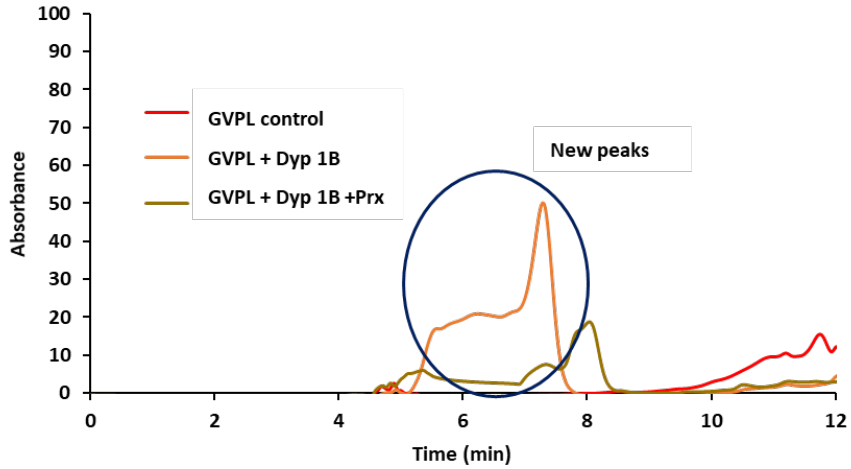

Figure S18. New product peaks from biotransformation of GVPL by Prx in combination with DyP 1B observed by reverse phase HPLC analysis.

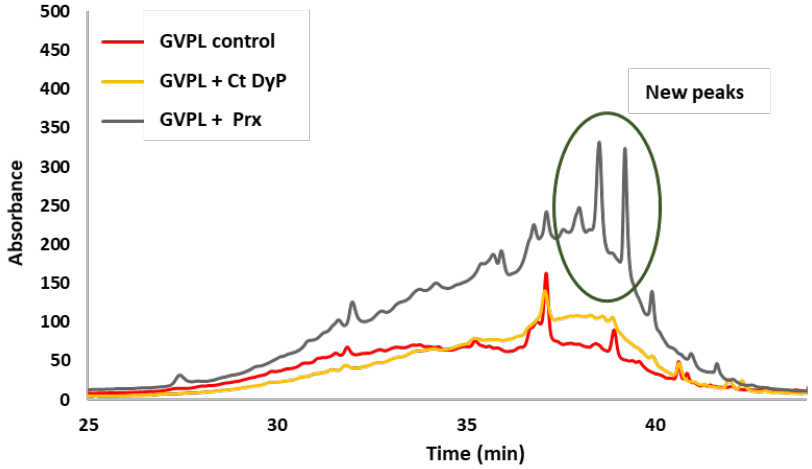

Figure S19. New product peaks from biotransformation of GVPL by Prx in combination with Ct DyP observed by reverse phase HPLC analysis.

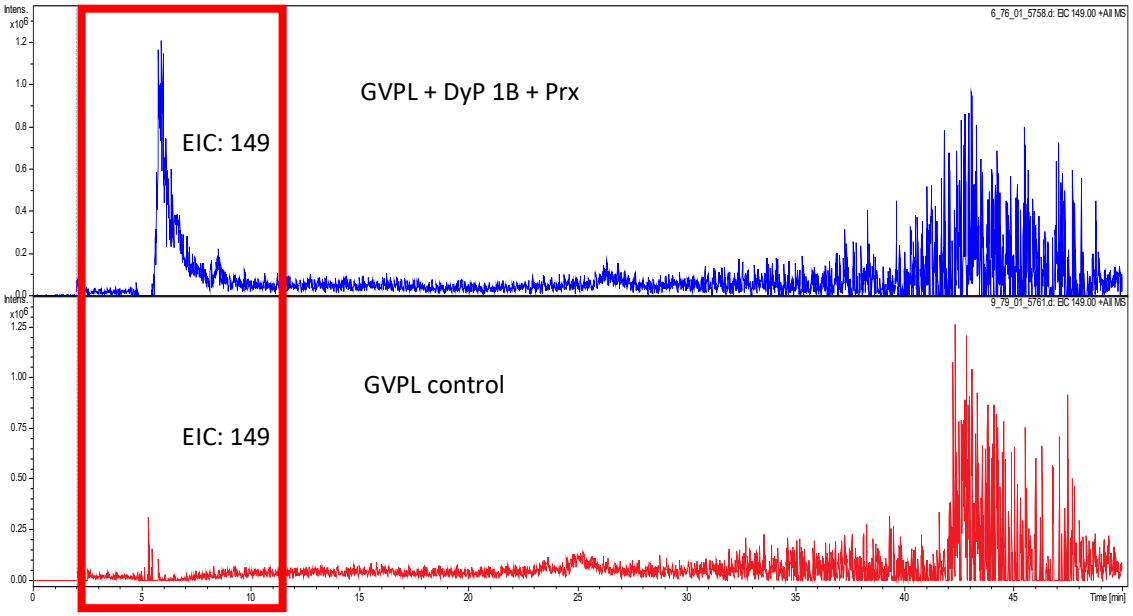

Figure S20. Incubation of GVPL with Dyp 1B enzyme in the presence of Prx, extracted ion chromatogram for *m/z* 149. Identified as 1-(4-hydroxyphenyl)ethanol (MH^+ 149) by comparison with commercial standard.

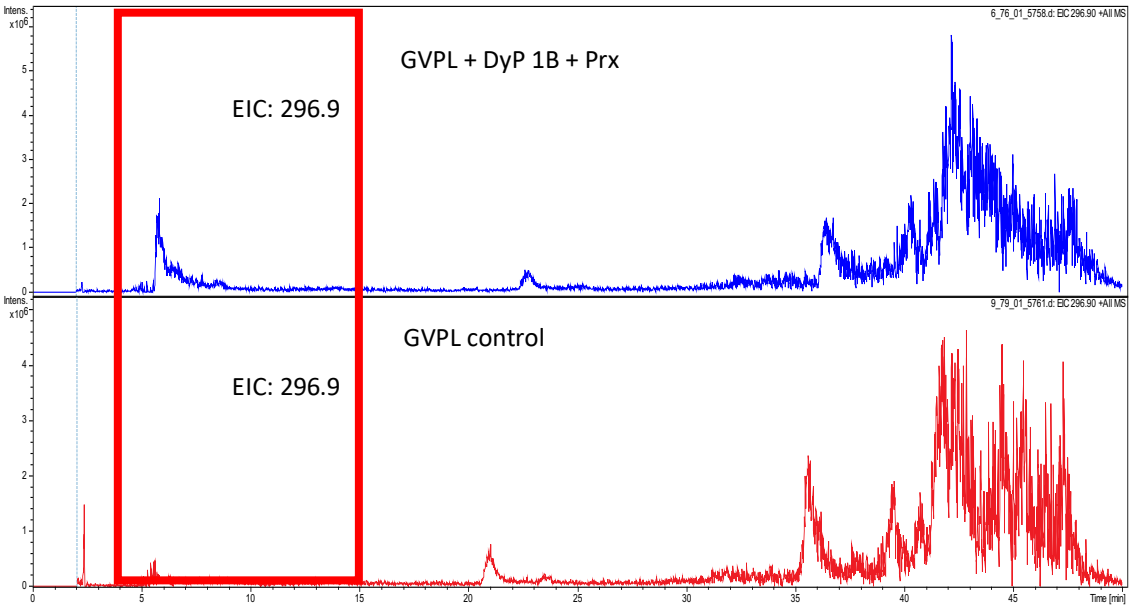

Figure S21. Incubation of GVPL with Dyp 1B enzyme in the presence of Prx, extracted ion chromatogram for *m/z* 296.9. Probable oxidised lignin dimer product (G,H units).

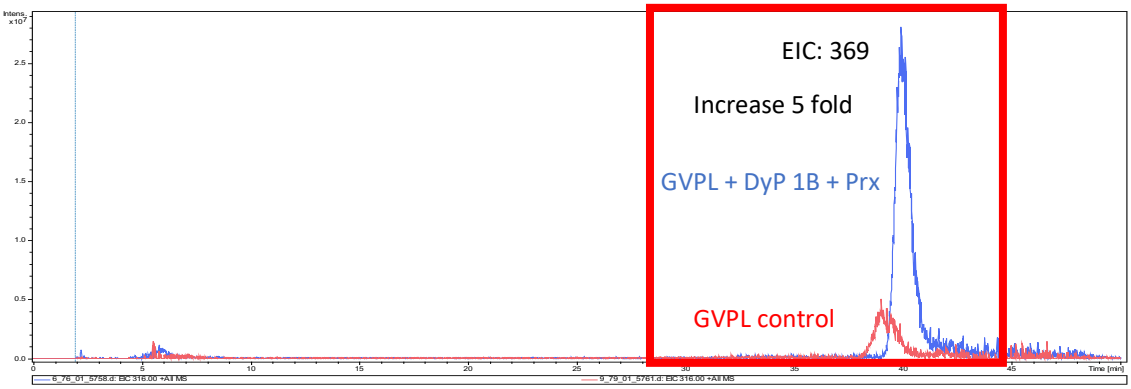

Figure S22. Incubation of GVPL with Dyp 1B enzyme in the presence of Prx, extracted ion chromatogram for *m/z* 369. Probable oxidised lignin dimer product (S,G units).

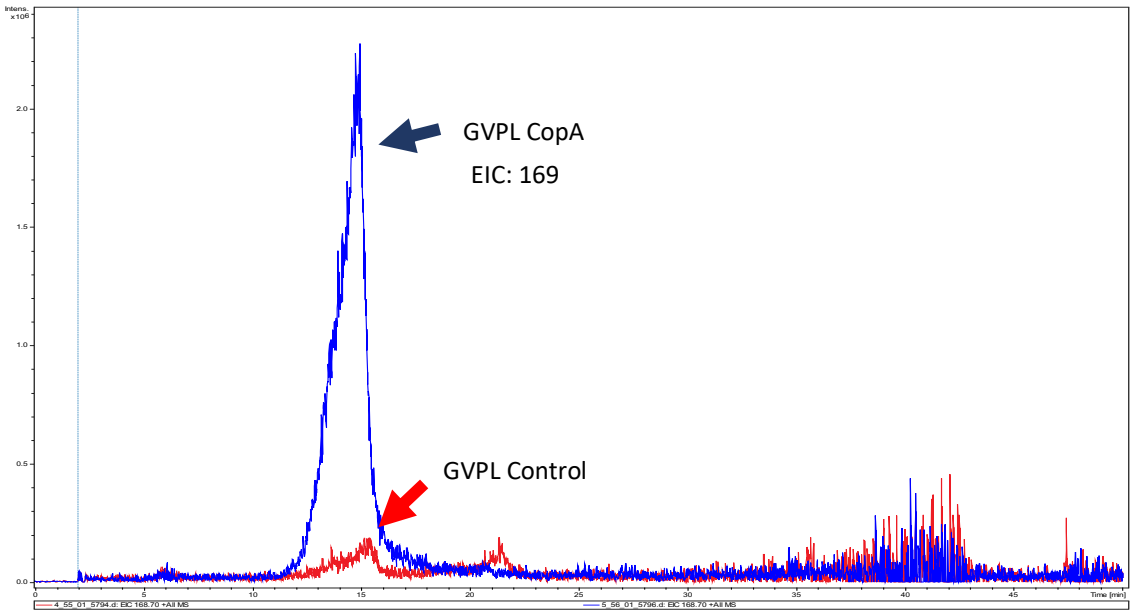

Figure S23. Incubation of GVPL with CopA enzyme, extracted ion chromatogram for *m/z* 169. Identified as vanillic acid (MH^+ 169) by comparison with commercial standard.

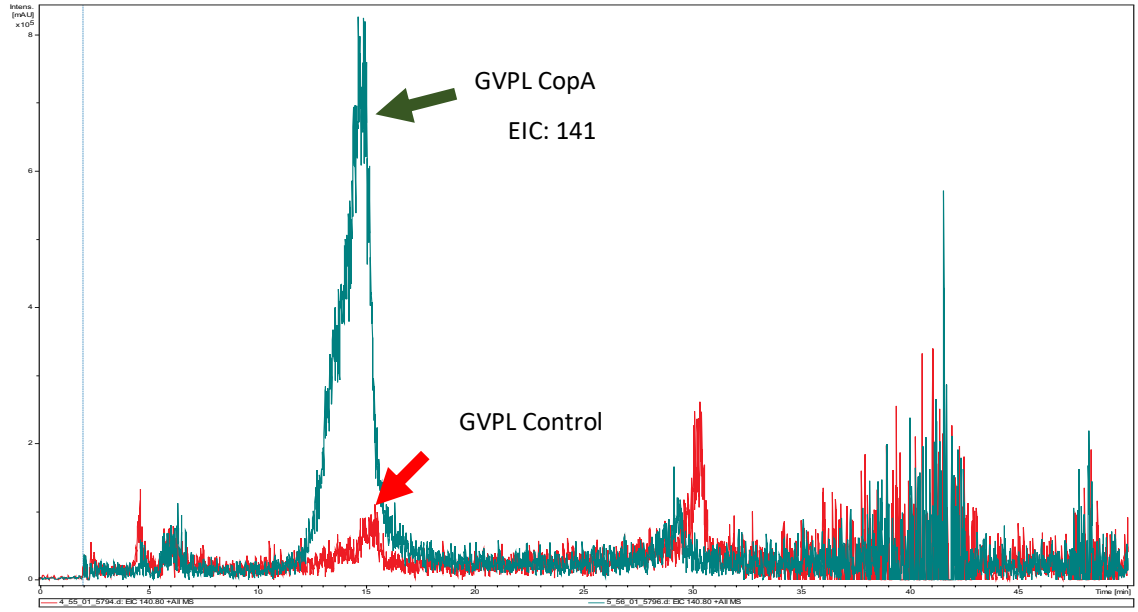

Figure S24. Incubation of GVPL with CopA enzyme, extracted ion chromatogram for *m/z* 141. Identified as methoxy-1,4-quinone (MH^+ 141) by comparison with commercial standard.

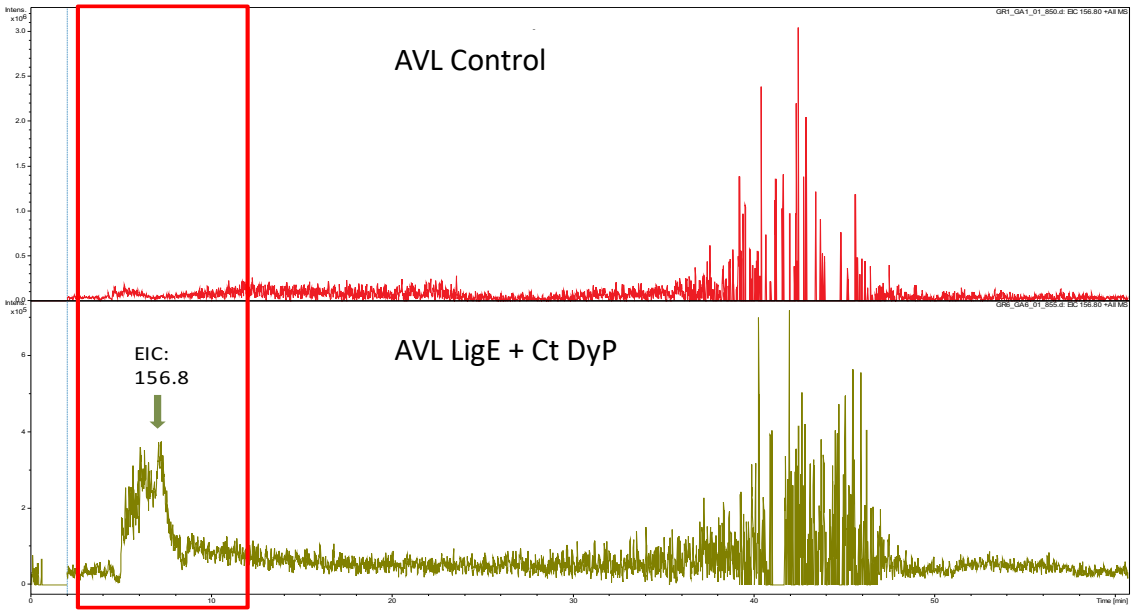

Figure S25. Incubation of AVL with CtDyp enzyme in the presence of LigE, extracted ion chromatogram for *m/z* 156.8. Structure not identified.

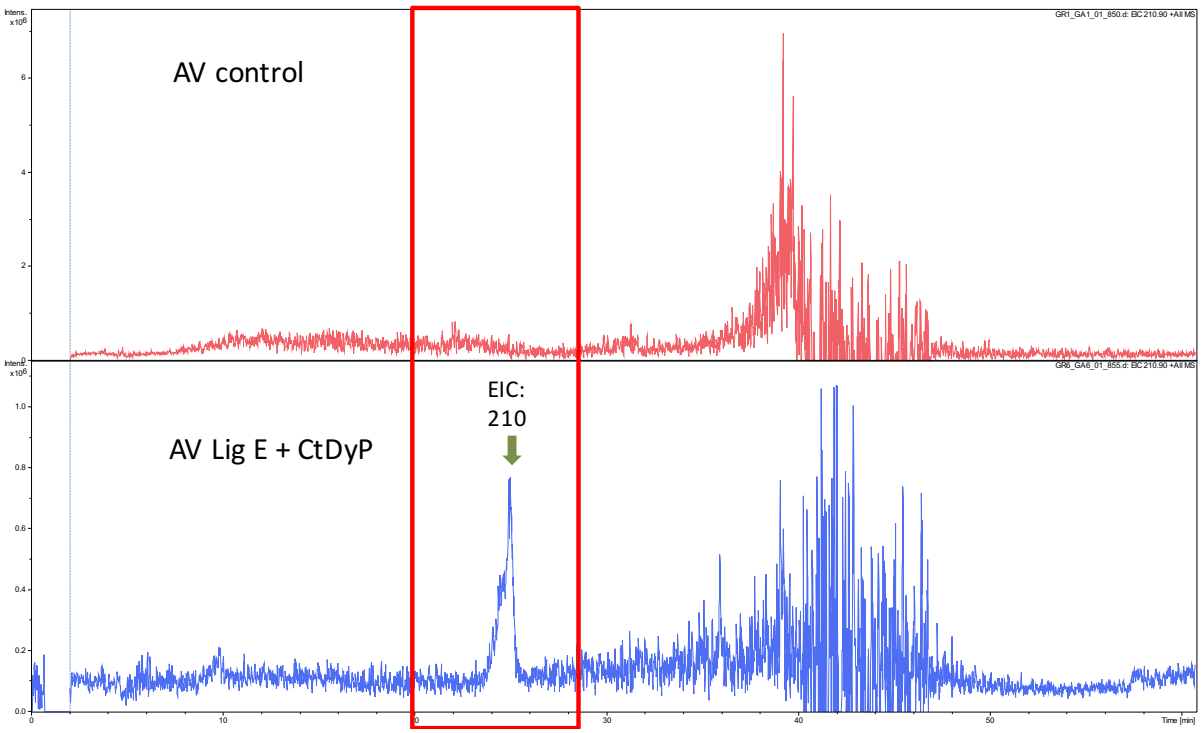

Figure S26. Incubation of AVL with Ct Dyp enzyme in the presence of LigE, extracted ion chromatogram for *m/z* 210. Co-eluted with 1-(4-hydroxy-3-methoxyphenyl)-1-oxo-propan-3-ol, identified in previous study (ref 22).

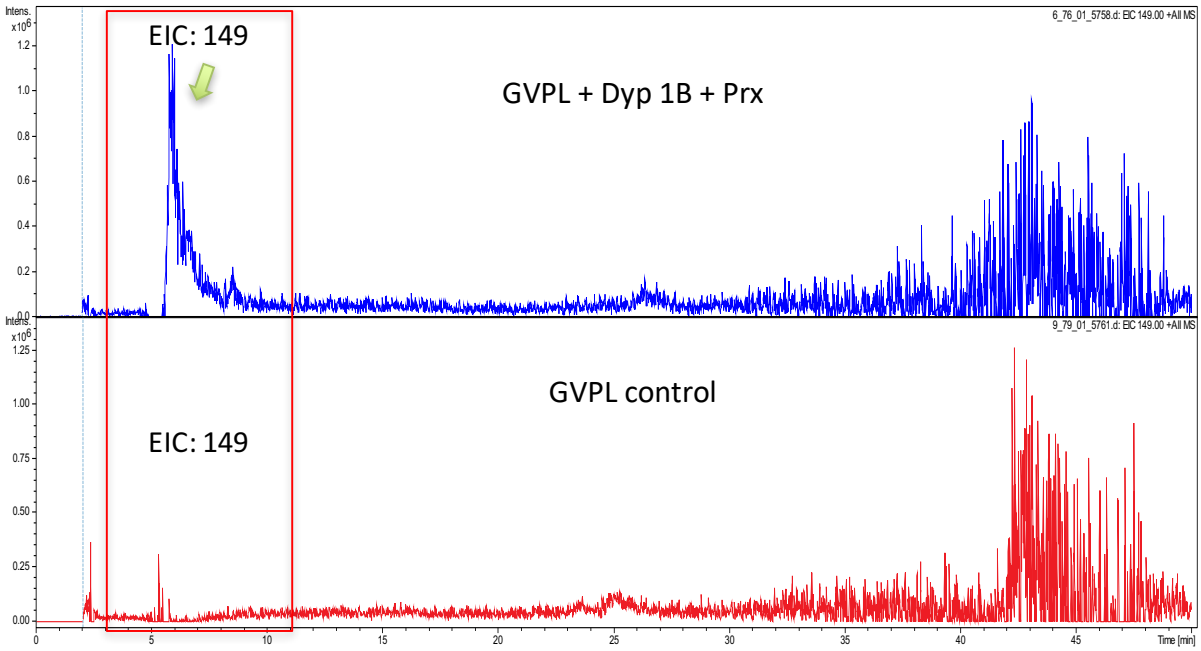

Figure S27. Incubation of GVPL with Dyp 1B enzyme in the presence of peroxiredoxin, extracted ion chromatogram for *m/z* 149. Identified as 1-(4-hydroxyphenyl)ethanol (MH^+ 149) by comparison with commercial standard.

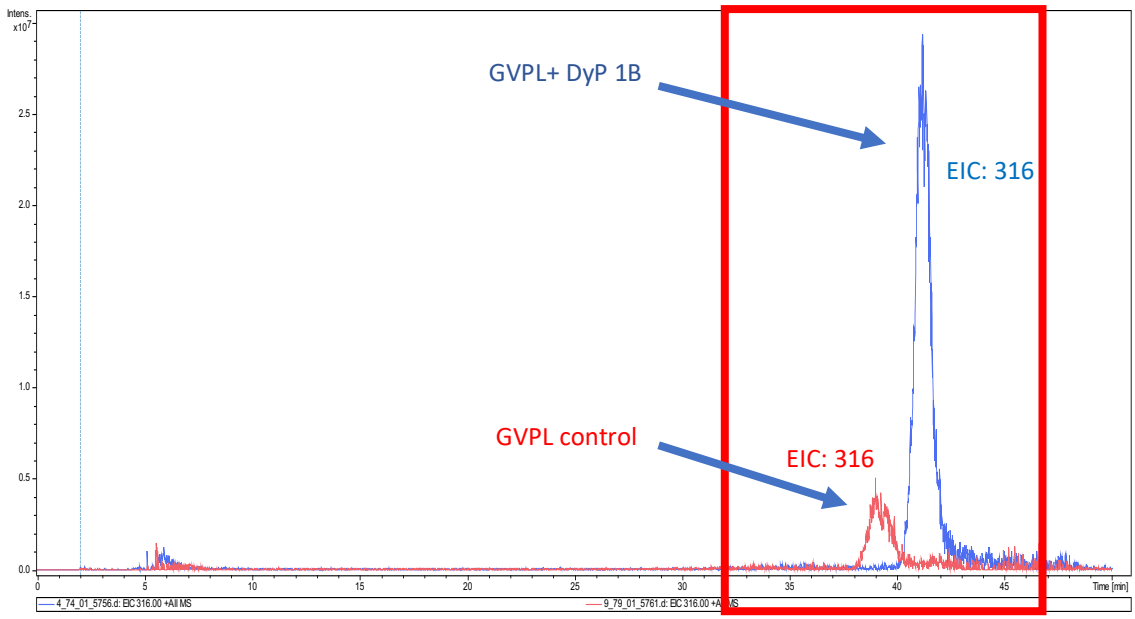

Figure S28. Incubation of GVPL with Dyp 1B enzyme, extracted ion chromatogram for *m/z* 316. Probable oxidised lignin dimer (G,G units).

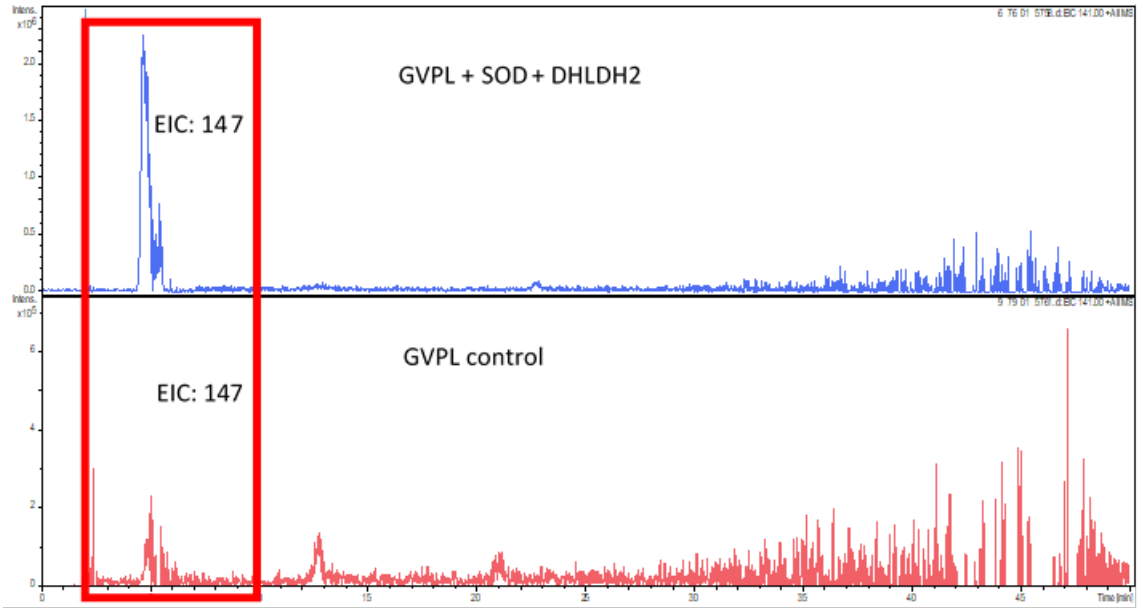

Figure S29. Incubation of GVPL with SOD enzyme in the presence of DHLDH2, extracted ion chromatogram for *m/z* 147. Identified as (4-hydroxyphenyl)methylketone (MH^+ 147) by comparison with commercial standard.

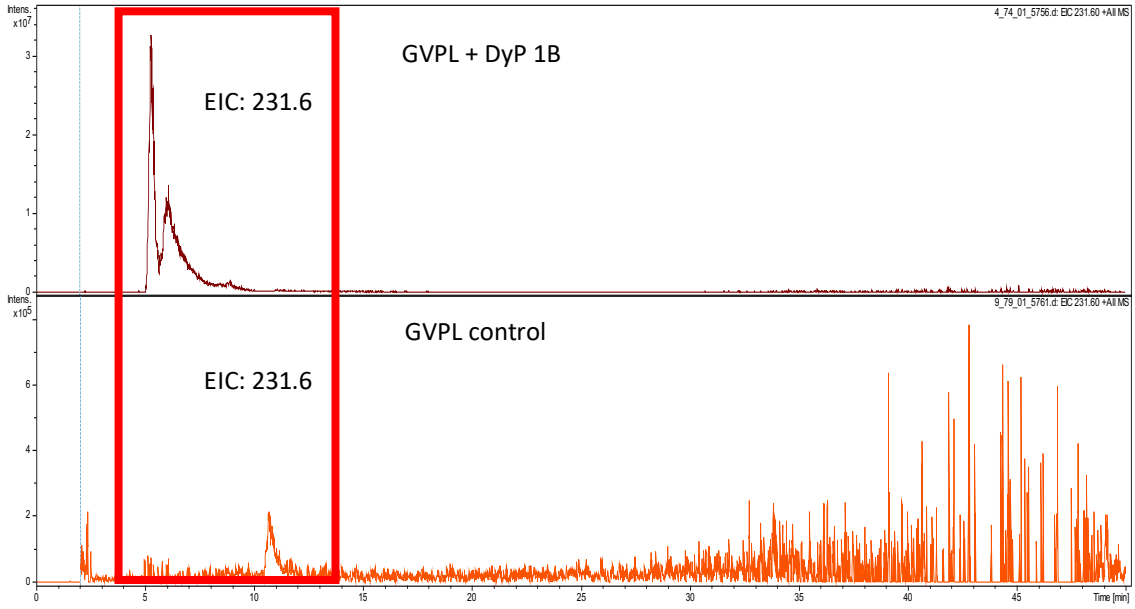

Figure S30. Incubation of GVPL with Dyp 1B enzyme, extracted ion chromatogram for *m/z* 231.6.

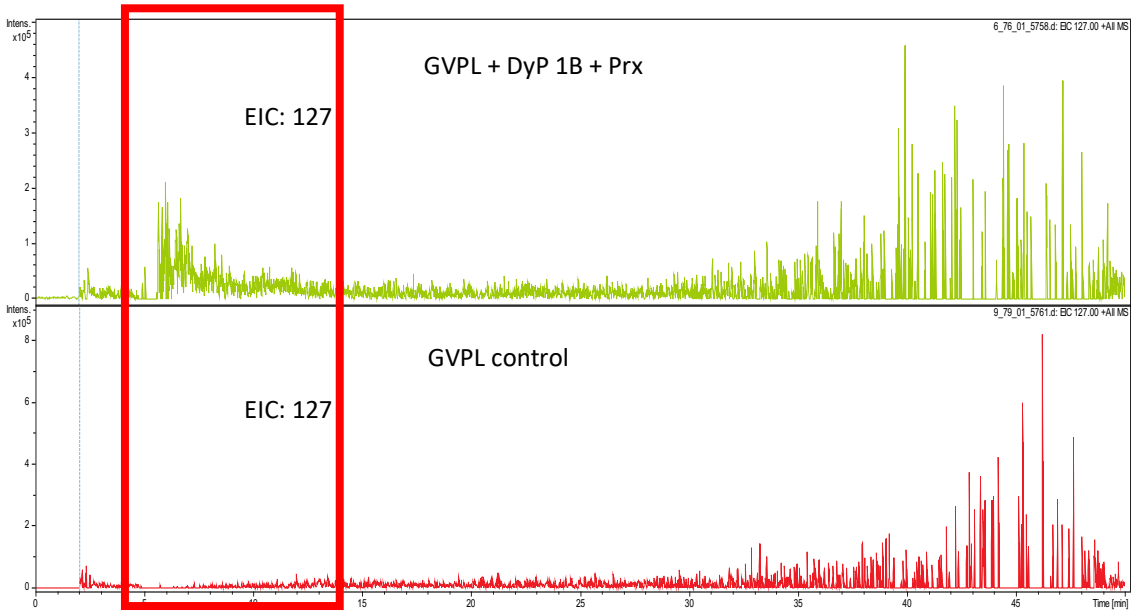

Figure S31. Incubation of GVPL with Dyp 1B enzyme in the presence of Peroxiredoxin, extracted ion chromatogram for *m/z* 127. Identified as hydroxyquinol (MH^+ 127) by comparison with commercial standard.

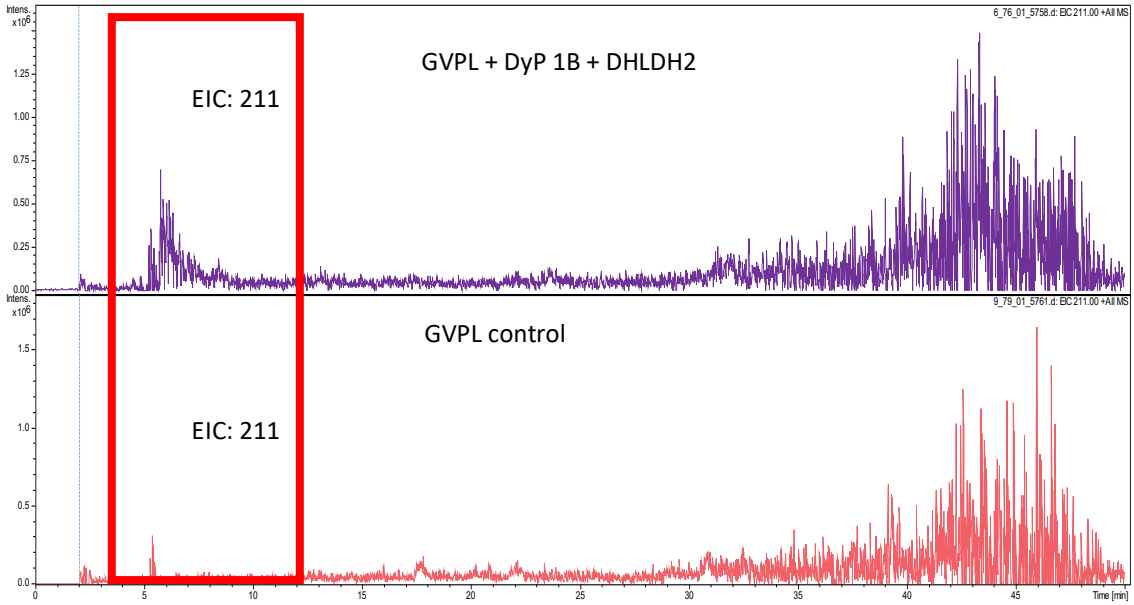

Figure S32. Incubation of GVPL with Dyp 1B enzyme in the presence of DHLDH2, extracted ion chromatogram for *m/z* 211. Structure assigned as 4-hydroxy-3-methoxyphenyl-propanediol (MH^+ 211) by similar elution profile with 4-hydroxy-3-methoxyphenyl-propanetriol observed in previous study (ref 22).

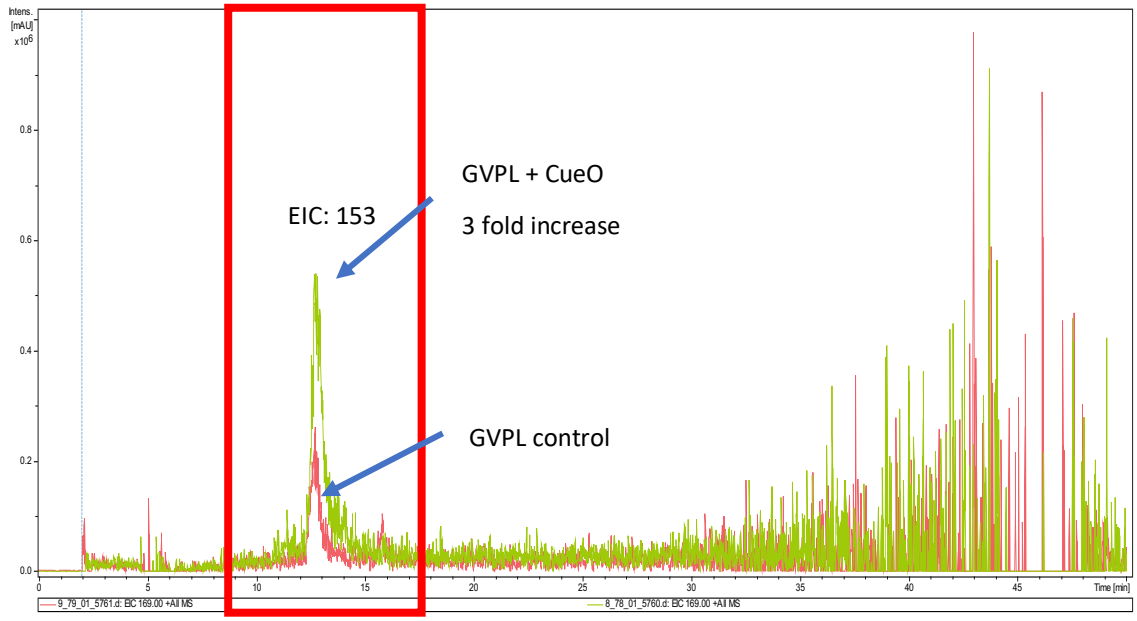

Figure S33. Incubation of GVPL with Dyp 1B enzyme, extracted ion chromatogram for *m/z* 153. Identified as vanillin (MH^+ 153) by comparison with commercial standard.